Supporting Information

Capsule self-oscillating gels showing cell-like nonthermal membrane/shape fluctuations

Won Seok Lee,[a] Takafumi Enomoto,[a] Aya Mizutani Akimoto,[a] and Ryo Yoshida[a*]

[a] Department of Materials Engineering, School of Engineering, The University of Tokyo

7-3-1 Hongo, Bunkyo-ku, Tokyo 113-8656, Japan

[1]Tel: +81-3-5841-7112, Fax: +81-3-5841-7112

E-mail: ryo@cross.t.u-tokyo.ac.jp

1. Experimental Procedures

1.1. Materials

N-isopropylacrylamide (NIPAAm) was kindly provided by KJ Chemicals (Tokyo, Japan) and purified by recrystallization in toluene/hexane. N-(3-aminopropyl)methacrylamide hydrochloride (NAPMAm) was purchased by Polyscience (Warrington, PA) and used as received. N,N'-methylenebisacrylamide (MBAAm), ammonium persulfate (APS), N,N,N',N'-tetramethylethylenediamine (TEMED), hexane, super dehydrated dimethyl sulfoxide (DMSO), sodium bromate ($NaBrO_3$), 1 M HNO_3 aqueous solution, malonic acid ($CH_2(COOH)_2$) (MA), sodium alginate (80 ~ 120 cP), calcium chloride ($CaCl_2$), sodium citrate, sodium chloride (NaCl), 5-aminofluorescein (Isomer I), N-hydroxysuccinimide (NHS), 1-(3-dimethylaminopropyl)-3-ethylcarbodiimide hydrochloride (EDC), sodium hydroxide (NaOH), and triethylamine (TEA) were purchased from Wako Pure Chemical Industries (Osaka, Japan). Silicon oil (KF-96-100 CS) was purchased from Shin-Estu Chemical co, Ltd. (Tokyo, Japan). Water used in this study was purified by a water purifier (WA200, Yamato Scientific, Tokyo, Japan). Bis(2,2'-bipyridine) (1-(4'-methyl-2,2'-bipyridine-4-carbonyloxy)-2,5-pyrrolidinedione) ruthenium(II) ($Ru(bpy)_3$-NHS) was purchased from Trylead Chemical (Hangzhou, China).

1.2. Fabrication of the Alg/Ca beads

A 2 % (w/v) sodium alginate aqueous solution was transferred to a syringe with an 18 gauge needle (inner diameter = 1.27 mm). Then, the sodium alginate solution was added drop-wise into a constantly stirred 0.5 M $CaCl_2$ aqueous solution using a syringe with a flow rate of 100 ml/h. After continuous stirring for 90 min, the alginate/calcium (Alg/Ca) beads were dialyzed against deionized water for three days.

1.3. Fabrication of the poly(NIPAAm-*co*-NAPMAm) capsule gels (CGs)

A poly(NIPAAm-*co*-NAPMAm)) gel layer was synthesized on the Alg/Ca beads surface, referring to the previous report.[1] The aqueous monomer solutions (4 ml) containing NIPAAm (808 mg, 95 mol%), NAPMAm (26.8 mg, 2 mol %), MBAAm (34.7 mg, 3 mol%), and TEMED (11.2 μL) were prepared, followed by Ar bubbling for 30 min at 0 °C in an ice bath. The Alg/Ca beads were immersed in an aqueous solution of 2 ml of APS (17.1 mg/ml). According to the necessary, the immersion time into the APS solutions was 10 min or more (see **Fig. 2**). After the soaking, the Alg/Ca beads were carefully collected and transferred to the monomer solution. During the immersion of the Alg/Ca beads into the monomer solutions, the monomer solutions were constantly stirred (300 rpm) at 23 °C to prevent the Alg/Ca beads from contacting the bottom of the reactor. The immersion times into the monomer solutions were varied to control the thickness of the synthesized gel layer (see **Fig. 2**). After the gelation, the capsule gels were carefully collected and washed with excessive deionized water several times. After that, to liquefy the core Alg/Ca beads, the capsule gels were put into a pH 8.5 sodium citrate solution and stirred for three days. The sodium citrate solution was exchanged every day. Then the gels were dialyzed in deionized water for a week; the deionized water was exchanged every day.

1.4. Fabrication of the capsule self-oscillating gels (C-SOGs)

The capsule gels were soaked in a super dehydrated DMSO containing TEA for 24 h at 23 °C. After that, the capsule gels were immersed in 0.5 ml of a super dehydrated DMSO solution containing TEA (6.96 μL) and Ru(bpy)$_3$-NHS (70 mM) at 45 °C for 24 h. During the immersion, Ru(bpy)$_3$-NHS was conjugated to the primary amine groups in NAPMAm. The capsule self-oscillating gels (C-SOGs) were dialyzed against DMSO 50 % aqueous solution for three days and deionized water for additional four days. The solvents during the dialysis were exchanged every day.

1.5. Geometric changes in the capsule self-oscillating gels (C-SOGs) in each redox state

The gels were equilibrated in the oxidized state (Ru(bpy)$_3^{3+}$) in an aqueous solution containing 894 mM HNO$_3$ and 84 mM NaBrO$_3$. Similarly, the gels were equilibrated in the reduced state (Ru(bpy)$_3^{2+}$) in an aqueous solution containing 894 mM HNO$_3$, 84 mM NaCl and 64 mM MA. Note that NaCl was added to maintain the ionic strength. The gel images were taken by an optical microscope (VHX 970F, Osaka, Japan). The geometrical elements, including the gel layer thickness and layer thickness-to-whole size ratio (T/S) (**Fig. 2**), were analyzed by the images taken by the ImageJ software (NIH, USA). The solid SOGs were also equilibrated in each redox state with the same conditions described in (**Fig. S6**).

1.6. Analysis of fluctuation behaviors during the BZ reaction

The gels were immersed in the catalyst-free BZ solution containing 894 mM HNO$_3$, 84 mM NaBrO$_3$, and 64 mM MA at 20 °C. During the BZ reaction, the gel images were taken with an optical microscope (VHX 970F, Osaka, Japan). The fluctuation behaviors were evaluated using ImageJ software (NIH, USA). The fluctuation behaviors in this study were classified into two groups: (1) multiple simultaneous layer thickness fluctuations (TFs) evaluated by layer thickness change (**Fig. 4**) and (2) two shape descriptors (aspect ratio and fluctuation deviation) evaluated by the gel shape changes (**Fig. 5**). We performed a one-way ANOVA with a Scheffe post-hoc method by Origin Pro 2022 to evaluate the statistical significance of the periods and the amplitudes of the shape descriptors, including aspect ratio and fluctuation deviation.

1.7. The retention test of alginate in the capsule gels after dissolving by the chelator

1.7.1. Synthesis of fluorescein-labeled alginate by EDC-NHS coupling

The 5-aminofluorescein-labeled alginate (AF-Alg) was synthesized at 23 °C by referring to the previous report (**Fig. S2(a)**).[2] A 2 % alginate solution was prepared by dissolving sodium alginate (1 g) in PBS solution (50 ml), and stirred until completely dissolved. Then, 1-Ethyl-3-(3-dimethylaminopropyl)carbodiimide (EDC) (300 mg) and N-hydroxysuccinimide (NHS) (150 mg) were added to the alginate solution and stirred for 2 hr. After that, 5-aminofluorescein (5 mg) was dissolved in the mixture, followed by stirring for 24 h. The solution was dialyzed in a dialysis membrane (MWCO 3.5 kDa) for a week. The external aqueous solvent was exchanged every day. After the dialysis, the final solution was freeze-dried. We note that all procedures were conducted in a darkroom without light.

1.7.2. Fabrication of fluorescein-labeled Alg/Ca (AF-Alg/Ca) beads

All procedures were the same as the processes described in the *Experimental Procedure 1.2* in the Supporting Information, except here a 2 % AF-Alg solution was used instead of the 2 % alginate solution. The image of the fabricated AF-Alg/Ca is displayed in **Fig. S2(b)**.

1.7.3. Synthesis of poly(NIPAAm-*co*-NAPMAm) layer on the AF-Alg/Ca beads

All procedures were the same as the processes described in the *Experimental Procedure 1.3* in the Supporting Information, except here AF-Alg/Ca beads were used instead of the Alg/Ca beads.

1.7.4. Liquifying the AF-Alg/Ca beads in the capsule gels

The capsule gels with fluorescein-labeled Alg/Ca beads in the core (AF-Alg/Ca capsule gels) were immersed in a stirred 0.1 M sodium citrate solution (**Fig. S2(c)**). The AF- Alg/Ca beads also followed the same process. Then we collected the entire external solution at a regular time interval, then added the same volume of the fresh sodium citrate solution. Some AF-Alg/Ca capsule gels were picked at the same time interval and observed by a fluorescence microscope (DFC 360FX, Leica, Mannheim, Germany). The AF-Alg/Ca beads were also observed by the fluorescence microscope.

1.8. Preparation of spherical solid poly (NIPAAm-*co*-NAPMAm) self-oscillating gels

The spherical solid poly(NIPAAm-*co*-NAPMAm) gels (solid SOGs) were synthesized by inverse suspension polymerization by dropping the pre-gel solution into silicon oil (**Fig. S5(a)**). The pre-gel solution was prepared by mixing (1) a monomer solution and (2) an initiator solution. Specifically, the monomer solution was prepared by dissolving NIPAAm (808 mg, 95 mol%), NAPMAm (26.8 mg, 2 mol%), MBAAm (34.7 mg, 3 mol%), and TEMED (11.2 μL) in deionized water (4.0 mL). (2) The initiator solution was made by dissolving APS (17.1 mg)

in deionized water (1.0 mL). Each solution was degassed by Ar bubbling while cooling it at 0 ℃ in an ice bath. Then the two solutions were mixed and immediately stirred vigorously by a vortex mixer. The mixed pre-gel solution was loaded into a syringe equipped with a 22G syringe needle (diameter 0.7 mm), then added dropwise to the stirred (100 rpm) silicone oil by a syringe pump (volume rate 75 ml/min). The distance between the surface of the silicone oil and the syringe needle was 20 cm. The batch was maintained at 25 ℃ for 3 hr under an Ar atmosphere for the gelation. After that, the gels were collected carefully, washed with hexane three times, and dialyzed with deionized water for a week. The spherical solid poly(NIPAAm-*co*-NAPMAm) self-oscillating gels were fabricated and dialyzed by the same method as C-SOGs described in *Experimental Procedure 1.4* in the Supporting Information. The imagage and the size distribution of fabricated gels are shown in **Fig. S5(b)** and **Fig. S5(c)**, respectively.

2. Supporting figures and notes

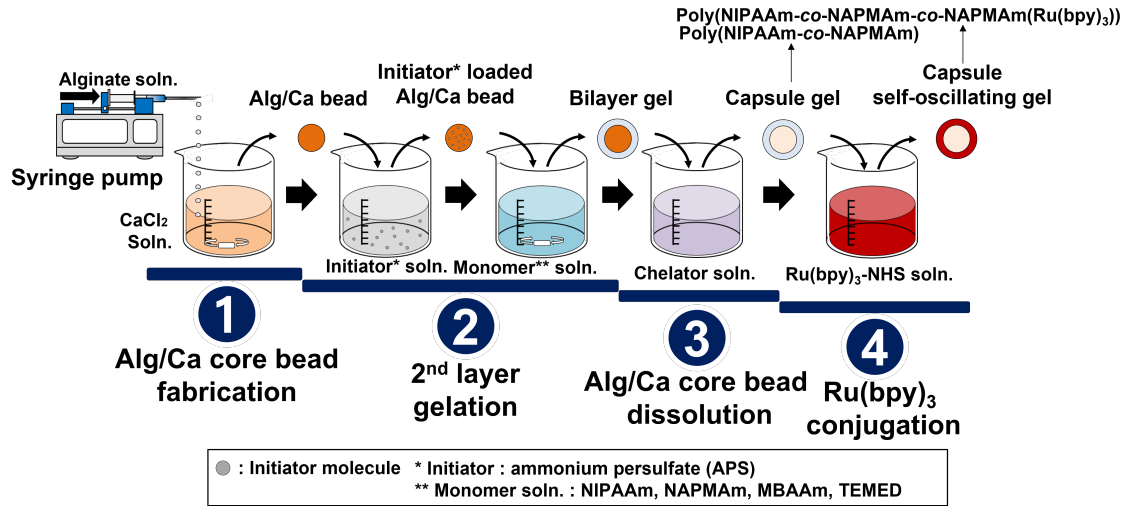### 2.1. Fabrication process of the capsule self-oscillating gels

Fig. S1. The detailed process for fabricating the capsule self-oscillating gels in this study.

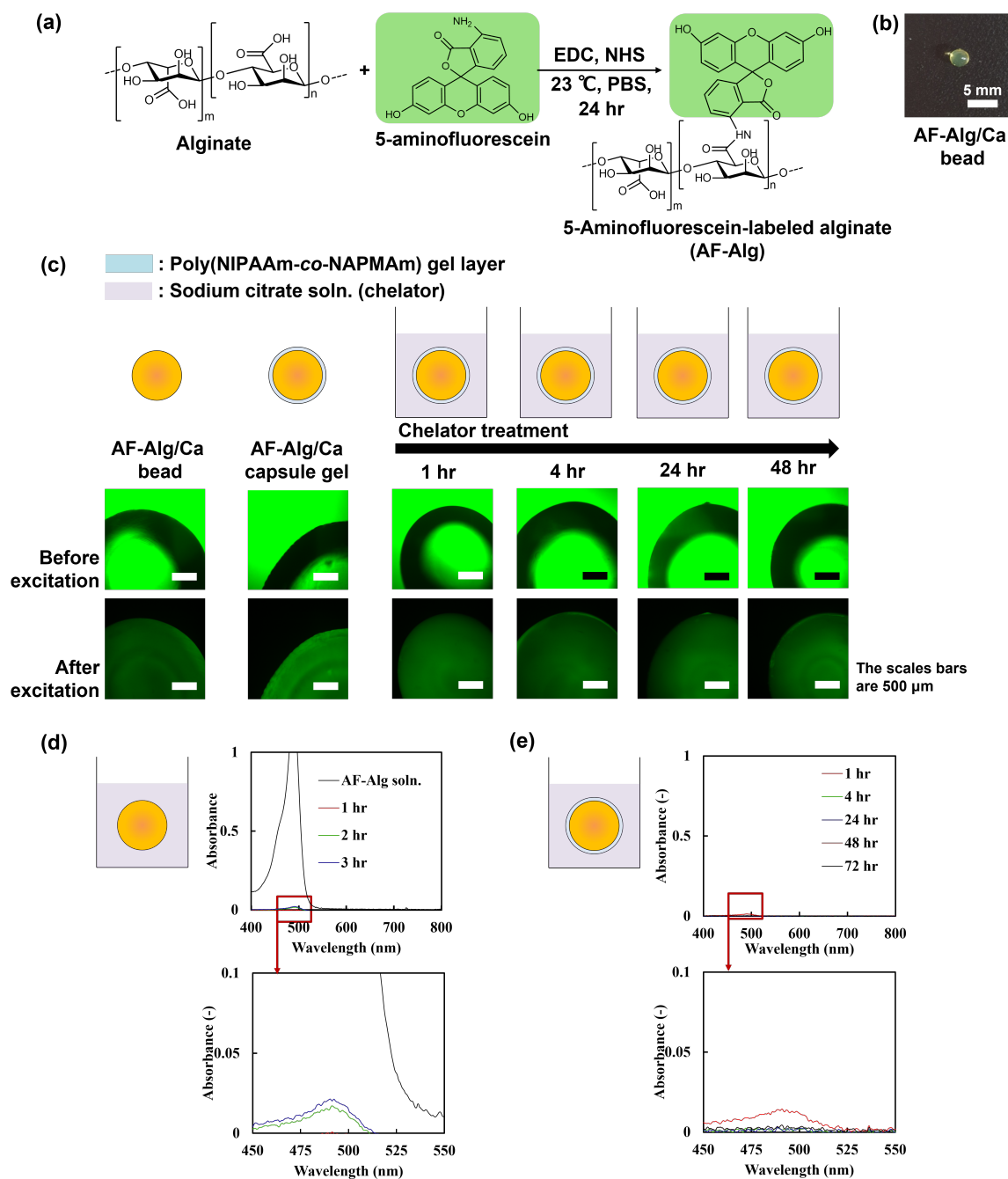## 2.2. The retention test of alginate in the capsule gels after dissolving by the chelator

Fig. S2 (a) The process for synthesizing fluorescein-labeled alginate (AF-Alg). (b) the image of fabricated fluorescein-labeled Alg/Ca (AF-Alg/Ca) bead. (c) fluorescent images of a AF-Alg/Ca bead and AF-Alg/Ca capsule gels (i.e., capsule gels with a poly(NIPAAm-*co*-NAPMAm) layer and inner AF-Alg/Ca core beads) over chelator treatment times. The gels were observed by a fluorescence microscope ($\lambda_{ex} = 494$ nm, $\lambda_{em} = 521$ nm) (DFC 360FX, Leica, Mannheim, Germany). (d) the UV-vis spectra of as follows: 2 % AF-Alg solution and the chelator solution obtained at regular intervals (i.e., 1 hr, 2 hr, and 3 hr) after the chelator treatment to the AF-Alg/Ca beads. (e) the UV-vis spectra of the chelator solution collected at regular intervals (i.e., 1 hr, 4 hr, 24 hr, 48 hr, and 72 hr) after the chelator treating of the AF-Alg/Ca capsule gels.

The carboxylic groups in the alginate can form unstable reactive o-acylisourea ester by reacting with EDC. The o-acylisourea ester can simultaneously react with NHS and form a semi-stable amine-reactive NHS ester. This NHS ester can react with the primary amine groups from 5-aminofluorescein, resulting in the AF-Alg. As shown in **Fig. S2(c)**, the fluorescent signal was detected in the AF-Alg/Ca beads as well as in the chelator-treated AF-Alg/Ca capsule gels, implying the AF-Alg retention inside the capsule structure. We also analyzed the collected external solutions by UV-vis spectroscopy (UV-2500PC, Shimadzu, Tokyo, Japan) to evaluate the leakage of the AF-Alg by the chelator treatment. As displayed in **Fig. S2(d)**, a weak signal was detected after 1 hr of chelator treatment, and the absorbance increased over time. We concluded that the Alg/Ca beads could start to be liquified 1 hr after chelator adding. **Fig. S2(e)** displays the absorbance changes over time of the chelator solutions containing the AF-Alg/Ca capsule gels. The signal was observed after 1 hr of the treatment but not detected over this time point. The results imply the following: at the initial stage of chelator treatment (e.g., 1 hr), a small amount of AF-Alg could be leaked from the core part. However, most of the liquified AF-Alg could not pass through the poly(NIPAAm-*co*-NAPMAm) gel layer and remained inside the capsule gel structure.

2.3. Mathematical modeling of the volume phase transition of the gels by redox state change

The measured geometric data (i.e., T/S values (**Fig. 3**) and the layer thickness (**Fig. S3**)) were mathematically fitted by the Boltzmann sigmoidal equation (**Eqn. (S1)**). Based on the fitted data, we calculated the difference in T/S values and the layer thickness in each redox state from approximately 10 °C to 35 °C (**Fig. S4**).

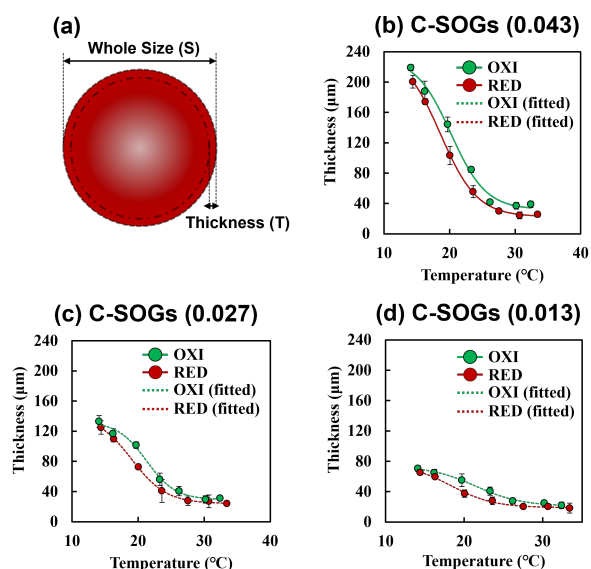$$y = \frac{A_1 - A_2}{1 + e^{x - x_0/dx}} + A_2 \qquad\qquad \textbf{Eqn. (S1)}$$

Fig. S3. (a) The schematic illustration describing the analyzed geometrical changes (thickness in this figure) in each redox state. The thickness changes as a function of the temperature in each redox state: the result of (b) C-SOGs (0.043), (c) C-SOGs (0.027), and (d) C-SOGs (0.013). The gels were immersed in the BZ substrate solution containing [HNO₃] = 894 mM and [NaBrO₃] = 84 mM for the oxidized state, and in [HNO₃] = 894 mM, [NaCl] = 84 mM, and [MA] = 64 mM for the reduced state. NaCl was added to maintain the ionic strength.

Table S1. Parameters resulting from mathematical modeling of the T/S value changes (see Fig. 3(b)-(d)), fitted by the Boltzmann sigmoidal equation. (OXI) indicates the oxidized state (Ru(bpy)$_3^{3+}$) while (RED) means the reduced state (Ru(bpy)$_3^{2+}$).

Sample	A_1	A_2	x_0	dx	R^2	Adj. R^2
C-SOGs (0.013) (OXI)	0.02369	0.00711	22.24981	2.51374	0.99272	0.98544
C-SOGs (0.013) (RED)	0.02345	0.00895	18.28597	2.48985	0.98920	0.97805
C-SOGs (0.027) (OXI)	0.05199	0.01148	21.45236	2.37737	0.99375	0.98750
C-SOGs (0.027) (RED)	0.05135	0.00924	19.1882	2.62898	0.99910	0.99820
C-SOGs (0.043) (OXI)	0.09975	0.01543	20.96392	2.55027	0.99366	0.98732
C-SOGs (0.043) (RED)	0.09742	0.00998	18.70957	2.87577	0.99960	0.99919

Table S2. Parameters resulting from mathematical modeling of the layer thickness changes (see Fig. S3(b)-(d)) fitted by the Boltzmann sigmoidal equation. (OXI) indicates the oxidized state ($Ru(bpy)_3^{3+}$) while (RED) means the reduced state ($Ru(bpy)_3^{2+}$).

| Sample	A_1	A_2	x_0	dx	R^2	Adj. R^2
C-SOGs (0.013) (OXI)	73.51837	21.0793	21.45873	2.90655	0.99597	0.99194
C-SOGs (0.013) (RED)	77.09640	18.86343	18.29880	2.75074	0.99598	0.99196
C-SOGs (0.027) (OXI)	132.39061	29.31355	21.25242	2.19173	0.99293	0.98586
C-SOGs (0.027) (RED)	141.58857	24.09942	19.01836	2.63463	0.99935	0.99871
C-SOGs (0.043) (OXI)	232.25547	32.07922	20.19490	2.66839	0.99342	0.98683
C-SOGs (0.043) (RED)	240.90290	22.55511	18.59001	2.81372	0.99970	0.99939
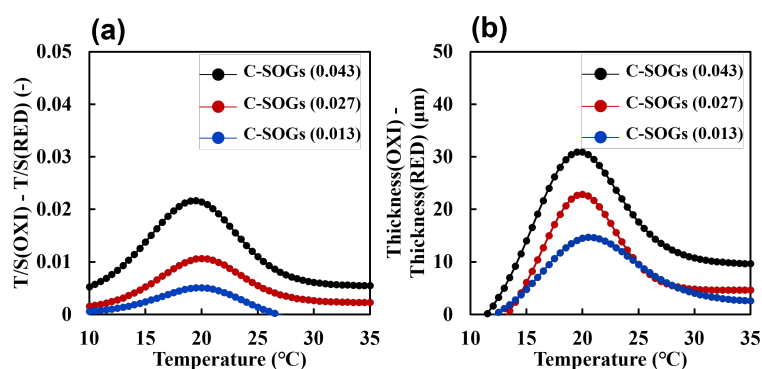
Fig. S4. The difference in (a) T/S and (b) layer thickness between the two redox states in the temperature range from 10 to 35 °C. Note that the analyzed gels were C-SOGs (0.043), C-SOGs (0.027), and C-SOGs (0.013), classified according to the T/S values in the reduced state at 20 °C. (OXI) indicates the oxidized state ($Ru(bpy)_3^{3+}$) while (RED) means the reduced state ($Ru(bpy)_3^{2+}$).

2.4. Preparation and equilibrium swelling behaviors of solid poly(NIPAAm-*co*-NAPMAm) self-oscillating gels

2.4.1. Preparation of spherical solid poly (NIPAAm-*co*-NAPMAm) self-oscillating gels
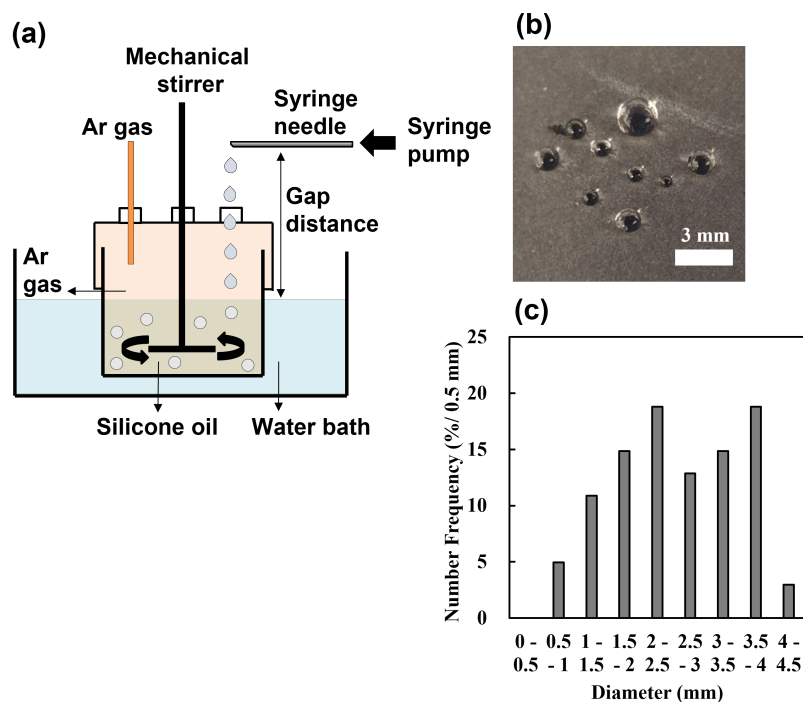

Fig. S5 (a) Schematic illustration of fabricating the spherical poly(NIPAAm-*co*-NAPMAm) solid gels. (b) the images of the solid fabricated poly(NIPAAm-*co*-NAPMAm) gels, and (c) the size distribution of the solid poly(NIPAAm-*co*-NAPMAm) gels according to the process described in this study. The images of the solid gels were taken by an optical microscope (VHX 970F, Keyence, Osaka, Japan).

2.4.2. Equilibrium swelling ratio of spherical solid poly(NIPAAm-*co*-NAPMAm) self-oscillating gels (solid SOGs)

The equilibrium swelling ratio indicates the diameter of the gels in each redox state at a specific temperature. The diameter of the spherical solid SOGs in each redox state was measured as a function of temperature. The equilibrium swelling ratio in **Fig. S6(a)** was calculated according to **Eqn. (S2)**. Diameter $(OXI)_{(L.T.)}$ indicates the gel diameter in the oxidized state (OXI) at the lowest temperature point (L.T.). Diameter (Redox state)$_{(T)}$ means the gel diameter in the corresponding redox state (Redox state) at the measured temperature point (T). The measured equilibrium swelling ratio was also fitted by Boltzmann Sigmoidal Equation (i.e., **Eqn. (S1))**.

$$Equilibrium\ Swelling\ Ratio = \frac{Diameter(Redox\ state)_{(T)}}{Diameter(OXI)_{(L.T.)}} \qquad \textbf{Eqn. (S2)}$$
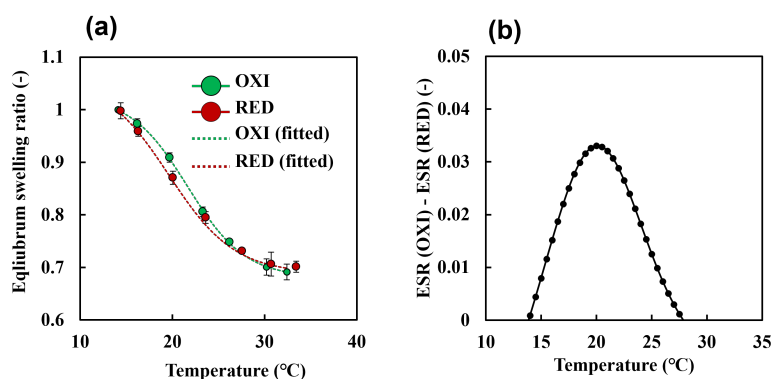

Fig. S6. (a) Equilibrium swelling ratio and fitted curve of the solid SOGs in each redox state as a function of the temperature. Concentrations of the BZ substrates: $[HNO_3]$ = 894 mM, $[NaBrO_3]$ = 84 mM for the oxidized state, and $[HNO_3]$ = 894 mM, $[NaCl]$ = 84 mM, $[MA]$ = 64 mM for the reduced state. NaCl was added to maintain the ionic strength. (b) The difference in the equilibrium swelling ratio between the redox states. The difference was calculated by utilizing the fitted curve. ESR indicates the equilibrium swelling ratio of the gels, (OXI) signifies the oxidized state $(Ru(bpy)_3^{3+})$ while (RED) means the reduced state $(Ru(bpy)_3^{2+})$.

Table S3. Parameters resulting from mathematical modeling of the equilibrium swelling ratio of the solid SOGs fitted by the Boltzmann sigmoidal equation. (OXI) indicates the oxidized state $(Ru(bpy)_3^{3+})$ while (RED) means the reduced state $(Ru(bpy)_3^{2+})$.

Sample	A_1	A_2	x_0	dx	R^2	Adj. R^2
Solid SOGs (OXI)	1.02679	0.68072	21.65177	3.11014	0.99970	0.99941
Solid SOGs (RED)	1.06272	0.68841	19.62003	3.56280	0.99831	0.99662

2.5. Calculation of period and amplitude during the BZ reaction

The period and the amplitude were quantitatively calculated to analyze the fluctuation behaviors. The period and amplitude were analyzed by **Eqn. (S3)** and **(S4)**, respectively, based on the profiles (**Fig. S7**). We note that the name and unit of the value (i.e., value$_{(top)}$ and value$_{(bottom)}$) in **Eqn. (S4)** could vary depending on the parameter to be measured.

$$Period\ (s) = Time_{post}(s) - Time_{pre}(s) \qquad \textbf{Eqn. (S3)}$$

$$Amplitude\ (unit) = Value_{top}(unit) - Value_{bottom}(unit) \qquad \textbf{Eqn. (S4)}$$
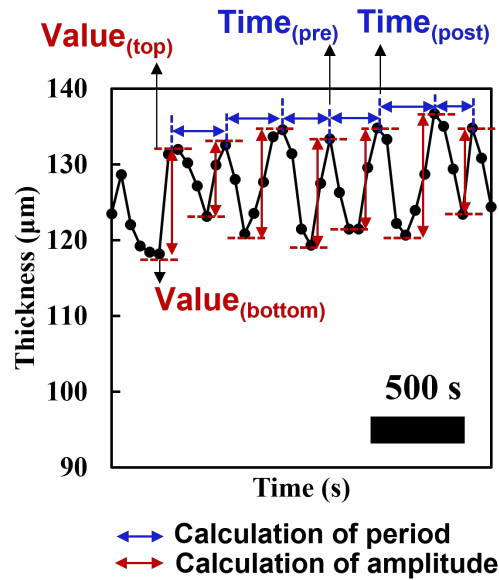

Fig. S7. Calculation of period and amplitude during the BZ reaction, related to Fig. 4-5. The analysis method of period and amplitude of the gels during the BZ reaction in this study at 20 °C. The thickness time profile of C-SOGs (0.043) in Region 3 (Fig. S8(b3)) is provided here as an example. Concentrations of the BZ substrates: [HNO$_3$] = 894 mM, [NaBrO$_3$] = 84 mM, and [MA] = 64 mM.

2.6. The detailed graphs displaying multiple simultaneous layer thickness fluctuations (TFs) during the BZ reaction
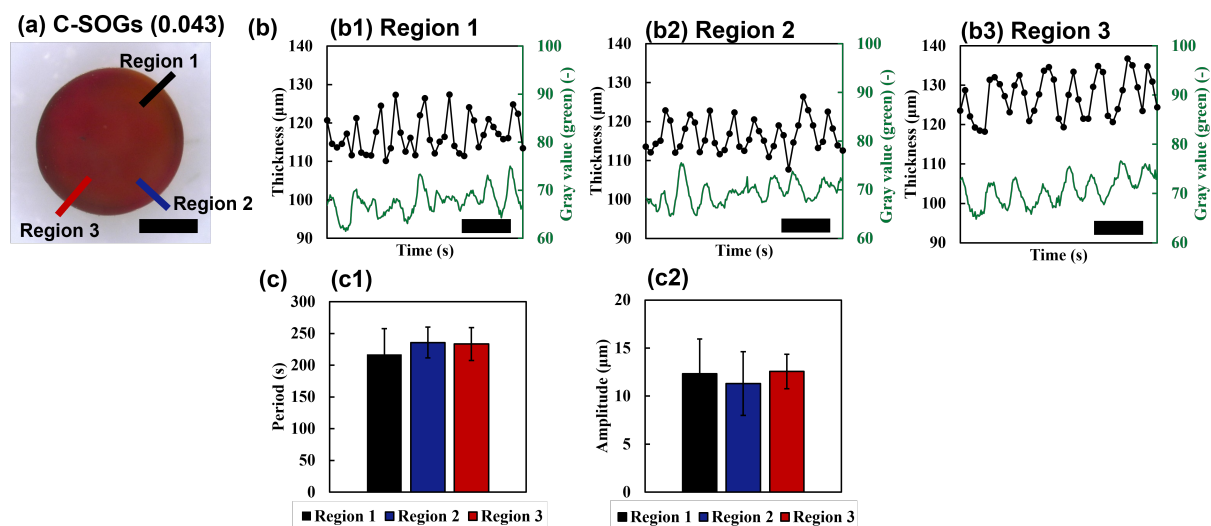

Fig. S8. The thickness fluctuations (TFs) of C-SOGs (0.043) during the BZ reaction at 20 °C. Concentrations of the BZ substrates: $[HNO_3]$ = 894 mM, $[NaBrO_3]$ = 84 mM, and $[MA]$ = 64 mM. (a) the image of the analyzed C-SOGs (same as Fig. 4(b1)) which also exhibits the analyzed regions; Region 1 (black line), Region 2 (blue line), and Region 3 (red line). The scale bar in (a) is 1 mm. The time profiles of the layer thickness and gray value (green channel) of Region 1 (b1), Region 2 (b2), and Region (b3). The scale bars in (b1)-(b3) are 500 s. The overlapped graphs for thickness profiles in all regions are shown in Fig. 4(b2), while gray values (green) are exhibited in Fig. 4(b3). The calculated periods from the layer thickness profiles in all regions are displayed in (c1), while the amplitudes are shown in (c2).

Fig. S9. The thickness fluctuations (TFs) of C-SOGs (0.027) during the BZ reaction at 20 °C. Concentrations of the BZ substrates: $[HNO_3]$ = 894 mM, $[NaBrO_3]$ = 84 mM, and $[MA]$ = 64 mM. (a1) the images of the analyzed C-SOGs taken at regular time intervals, and (a2) the gray-scale images (red channel) at the same time intervals. The red arrows indicate the oxidized point caused by the propagating BZ chemical wave. (b) the representative image of the C-SOGs (0.027), which also exhibits the analyzed regions; Region 1 (black line), Region 2 (blue line), and Region 3 (red line). The scale bars in (a) and (b) are 1 mm. The time profiles of the layer thickness and gray value (green channel) of Region 1 (c1), Region 2 (c2), and Region (c3). The scale bars in (c) are 500 s. The overlapped graphs for thickness profiles in all regions are shown in Fig. 4(c2), while gray values (green) are exhibited in Fig. 4(c3). The calculated periods from the layer thickness profiles in all regions are displayed in (d1), while the amplitudes are shown in (d2).
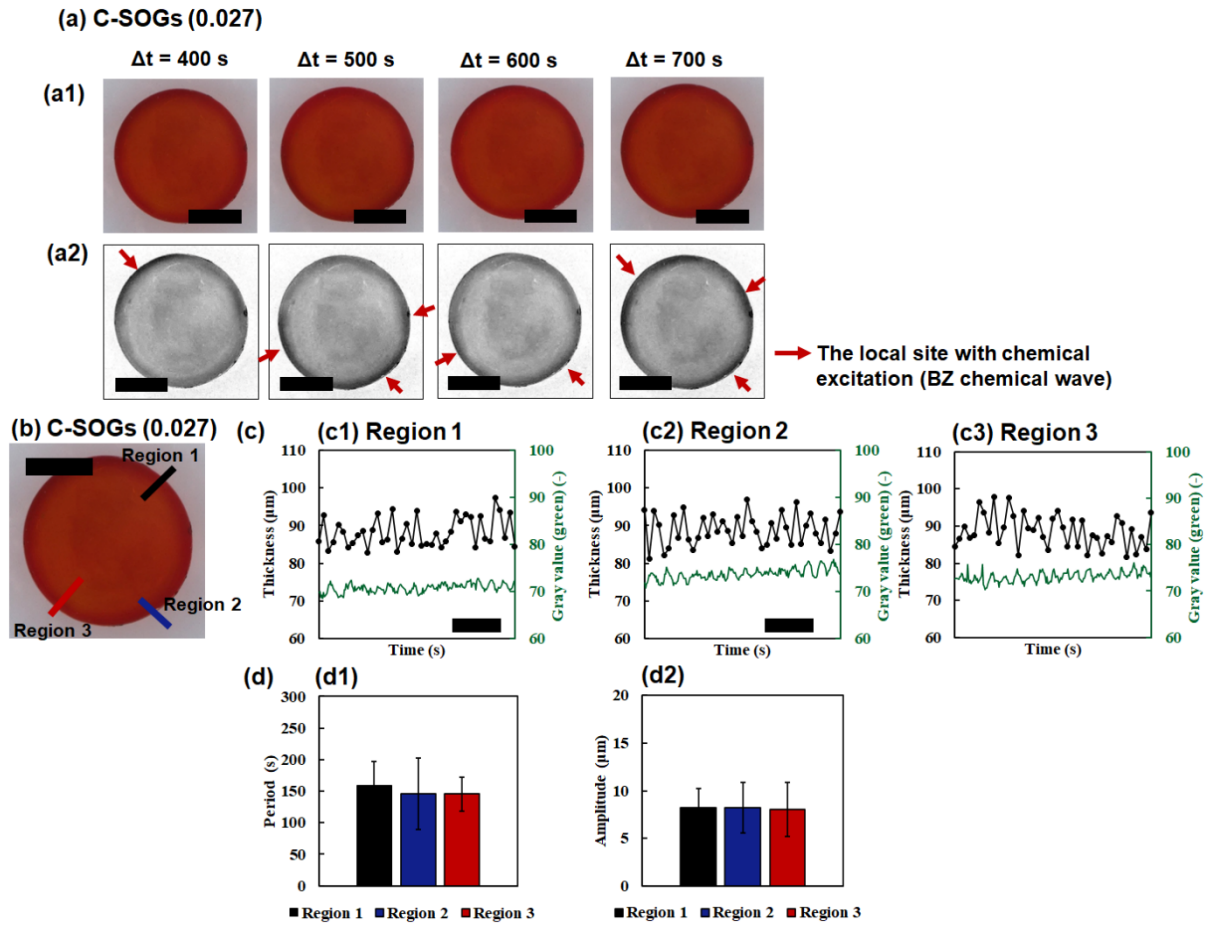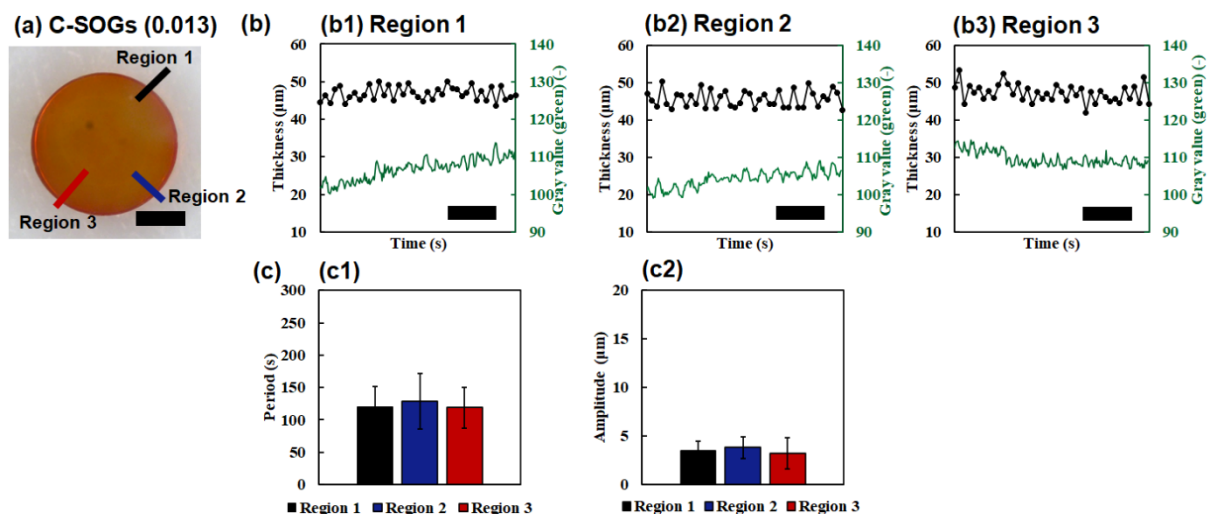
Fig. S10. The thickness fluctuations (TFs) of C-SOGs (0.013) during the BZ reaction at 20 °C. Concentrations of the BZ substrates: $[HNO_3]$ = 894 mM, $[NaBrO_3]$ = 84 mM, and $[MA]$ = 64 mM. (a) the image of the analyzed C-SOGs, which also exhibits the analyzed regions; Region 1 (black line), Region 2 (blue line), and Region 3 (red line). The scale bar in (a) is 1 mm. The time profiles of the layer thickness and gray value (green channel) of Region 1 (b1), Region 2 (b2), and Region (b3). The scale bars in (b) are 500 s. The overlapped graphs for thickness profiles in all regions are shown in Fig. 4(d2), while gray values (green) are exhibited in Fig. 4(d3). The calculated periods from the layer thickness profiles in all regions are displayed in (c1), while the amplitudes are shown in (c2). Note that we did not provide the gray value images (red channel) because the images could not display a visibly significant difference when a local part was oxidized.

2.7. Shape fluctuations (SFs) of the non-capsule solid self-oscillating gels (solid SOGs)
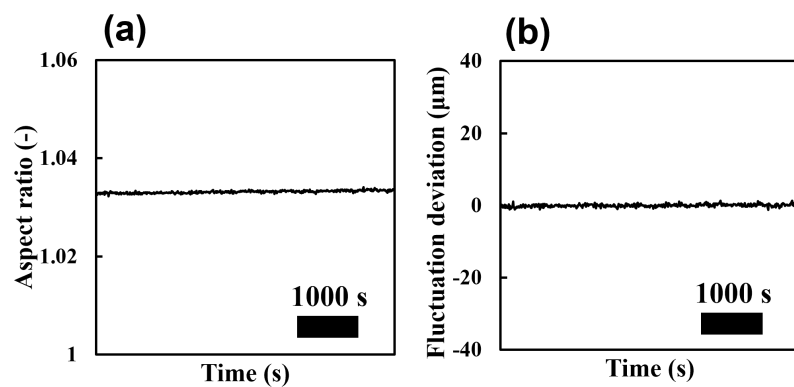

Fig. S11. Time profiles of the aspect ratio (a) and (b) the fluctuation deviation of the solid SOGs at 20 °C. Concentrations of the BZ substrates: $[HNO_3]$ = 894 mM, $[NaBrO_3]$ = 84 mM, and $[MA]$ = 64 mM.

2.8. Statistics of the C-SOGs shape fluctuations (SFs)

The statistics elements of the shape descriptors reflecting SFs during the BZ reaction at 20 °C are listed in **Tables S4-7**. The shape descriptors in this study indicate the aspect ratio and the fluctuation deviation. The statistics elements were from the box and whisker plots (**Fig. 5(d) and (e)**).

Table S4. The elements of the box and whisker plot corresponding to the period of aspect ratio (Fig. 5(d1)) during the BZ reaction at 20 °C.

Statistics	C-SOGs (0.043)	C-SOGs (0.027)	C-SOGs (0.013)
Upper outlier (s)	430	-	-
Maximum (s)	430	210	180
Third quartile (Q3) (s)	320	180	130
Mean (s)	280	163	112
Median (s)	280	160	110
First quartile (Q1) (s)	250	150	90
Interquartile range (IQR) (Q3-Q1) (s)	60	30	40
Minimum (s)	130	110	30
Lower outlier (s)	130	-	-

Table S5. The elements of the box and whisker plot corresponding to the amplitude of the aspect ratio (Fig. 5(d2)) during the BZ reaction at 20 °C.

Statistics	C-SOGs (0.043)	C-SOGs (0.027)	C-SOGs (0.013)
Upper outlier	-	-	-
Maximum	1.36×10^{-2}	1.17×10^{-2}	0.66×10^{-2}
Third quartile (Q3)	0.97×10^{-2}	0.84×10^{-2}	0.31×10^{-2}
Mean	0.70×10^{-2}	0.65×10^{-2}	0.25×10^{-2}
Median	0.69×10^{-2}	0.63×10^{-2}	0.23×10^{-2}
First quartile (Q1)	0.61×10^{-2}	0.46×10^{-2}	0.12×10^{-2}
Interquartile range (IQR) (Q3-Q1)	0.36×10^{-2}	0.39×10^{-2}	0.19×10^{-2}
Minimum	0.53×10^{-2}	0.43×10^{-2}	0.20×10^{-2}
Lower outlier	-	-	-

Table S6. The elements of the box and whisker plot corresponding to the period of fluctuation deviation (Fig. 5(e1)) during the BZ reaction at 20 °C.
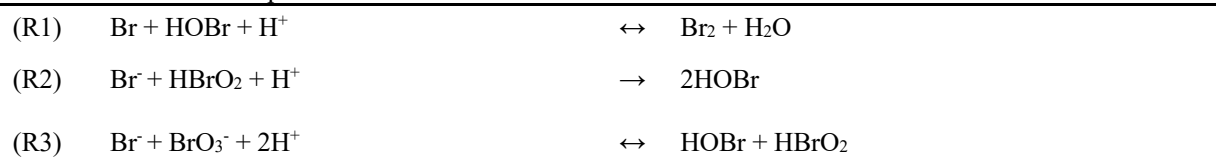
Statistics	C-SOGs (0.043)	C-SOGs (0.027)	C-SOGs (0.013)
Upper outlier (s)	-	-	-
Maximum (s)	380	220	180
Third quartile (Q3) (s)	320	180	130
Mean (s)	300	165	103
Median (s)	295	160	100
First quartile (Q1) (s)	280	150	70
Interquartile range (IQR) (Q3-Q1) (s)	40	30	60
Minimum (s)	240	110	40
Lower outlier (s)	-	-	-

Table S7. The elements of the box and whisker plot corresponding to the amplitude of fluctuation deviation (Fig. 5(e2)) during the BZ reaction at 20 °C.
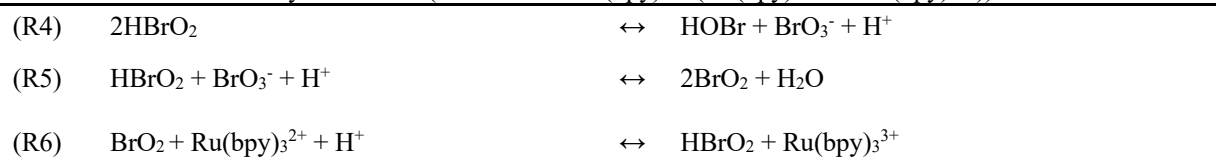
Statistics	C-SOGs (0.043)	C-SOGs (0.027)	C-SOGs (0.013)
Upper outlier (μm)	-	-	-
Maximum (μm)	33.6	34.1	20.9
Third quartile (Q3) (μm)	28.3	24.1	9.81
Mean (μm)	22.7	19.2	7.10
Median (μm)	22.5	17.0	6.52
First quartile (Q1) (μm)	18.0	14.0	4.32
Interquartile range (IQR) (Q3-Q1) (μm)	10.3	10.1	5.49
Minimum (μm)	11.0	4.56	0.38
Lower outlier (μm)	-	-	-

2.9. The effect of initial BZ substrate concentration on the shape fluctuations (SFs)

Process A: consumption of bromide ion

(R1)	$Br + HOBr + H^+$	$\leftrightarrow$	$Br_2 + H_2O$
(R2)	$Br^- + HBrO_2 + H^+$	$\rightarrow$	$2HOBr$
(R3)	$Br^- + BrO_3^- + 2H^+$	$\leftrightarrow$	$HOBr + HBrO_2$

Process B: autocatalytic reaction (oxidation of $Ru(bpy)_3^{2+}$ ($Ru(bpy)_3^{2+} \rightarrow Ru(bpy)_3^{3+}$))

(R4)	$2HBrO_2$	$\leftrightarrow$	$HOBr + BrO_3^- + H^+$
(R5)	$HBrO_2 + BrO_3^- + H^+$	$\leftrightarrow$	$2BrO_2 + H_2O$
(R6)	$BrO_2 + Ru(bpy)_3^{2+} + H^+$	$\leftrightarrow$	$HBrO_2 + Ru(bpy)_3^{3+}$

Process C: production of bromomalonic acid (reduction of $Ru(bpy)_3^{3+}$ ($Ru(bpy)_3^{3+} \rightarrow Ru(bpy)_3^{2+}$))

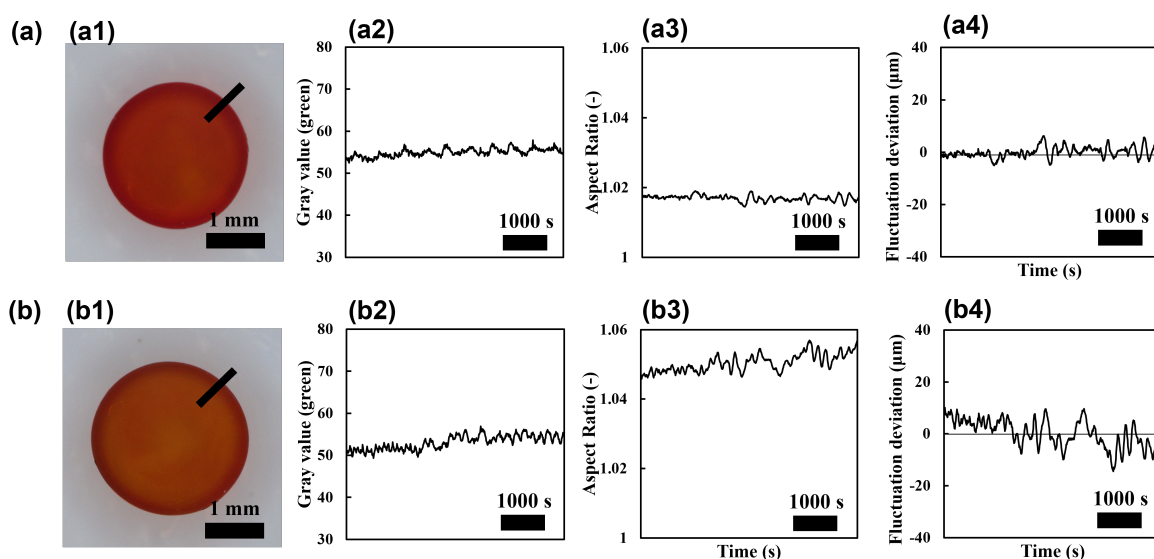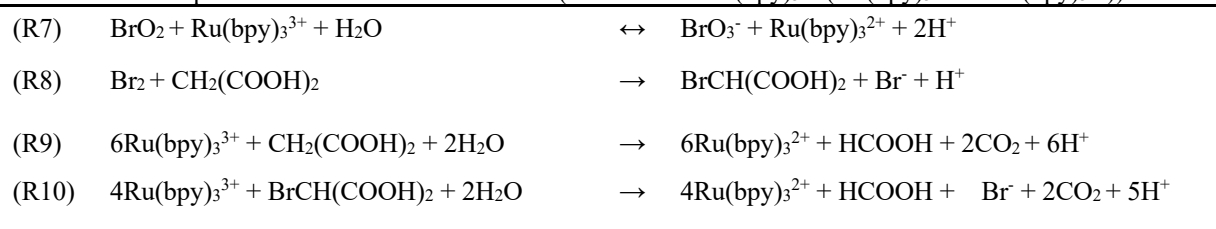| (R7)	$BrO_2 + Ru(bpy)_3^{3+} + H_2O$	$\leftrightarrow$	$BrO_3^- + Ru(bpy)_3^{2+} + 2H^+$
(R8)	$Br_2 + CH_2(COOH)_2$	$\rightarrow$	$BrCH(COOH)_2 + Br^- + H^+$
(R9)	$6Ru(bpy)_3^{3+} + CH_2(COOH)_2 + 2H_2O$	$\rightarrow$	$6Ru(bpy)_3^{2+} + HCOOH + 2CO_2 + 6H^+$
(R10)	$4Ru(bpy)_3^{3+} + BrCH(COOH)_2 + 2H_2O$	$\rightarrow$	$4Ru(bpy)_3^{2+} + HCOOH + Br^- + 2CO_2 + 5H^+$

Fig. S12. Data that reveals the BZ substrate concentration-dependency of SFs during the BZ reaction at 20 °C. C-SOGs (0.027) with the following BZ substrate concentration were analyzed: (a) [HNO$_3$] = 894 mM, [NaBrO$_3$] = 42 mM, and [MA] = 64 mM, and (b) [HNO$_3$] = 894 mM, [NaBrO$_3$] = 84 mM, and [MA] = 32 mM. (a1 and b1) the images taken during the BZ reaction of the corresponding substrate conditions. (a2 and b2) Time profiles showing the gray value (green) change with the corresponding substrate conditions. The gray value (green) profiles were evaluated in the region with black lines shown in (a1) and (b1). (a3 and b3) Time profiles displaying the aspect ratio change of the corresponding substrate conditions. (a4 and b4) Time profiles exhibiting the fluctuation deviation changes of the corresponding substrate conditions.

We analyzed the effect of initial BZ substrate concentration on the SFs on the C-SOGs. The BZ substrate, including $NaBrO_3$ and MA, can affect the oscillatory behaviors of the BZ reaction and SOGs[3,4]. To confirm the specific effect, we selected the C-SOGs (0.027) as a representative model and varied the concentration of sodium bromate (**Fig. S12(a)**) and MA (**Fig. S12(b)**). In specific, the typical substrate concentration in the manuscript was as follows: $[HNO_3]$ = 894 mM, $[NaBrO_3]$ = 84 mM, and [MA] = 64 mM, while the data in **Fig. S12(a)** was $[HNO_3]$ = 894 mM, $[NaBrO_3]$ = 42 mM, and [MA] = 64 mM, and **Fig. S12(b)** was $[HNO_3]$ = 894 mM, $[NaBrO_3]$ = 84 mM, and [MA] = 32 mM. We confirmed the period of gray value (green) in the region with a black line (**Fig. S12(a1)** and **(b1)**) which is the same as Region 1 in the manuscript. As shown in **Fig. S12(a2)**, when the $NaBrO_3$ concentration decreased, the period of the gray value oscillation increased (i.e., ~ 390 s) than that of the typical conditions (i.e., ~ 140 s in **Fig. S9(d)**). The aspect ratio (**Fig. S12(a3)**) and the fluctuation deviation (**Fig. S12(a4)**) changes were smaller than those of the typical condition in **Table 1** (**Fig. 5(b3)** and **(c3)**). When the MA concentration decreased, the period of gray value in the black-lined region slightly increased (i.e., ~ 170 s) more than the typical condition (i.e., ~ 140 s in **Fig. S9(d)**). The aspect ratio (**Fig. S12(b3)**) and the fluctuation deviation (**Fig. S12(b4)**) changes also fluctuated less than those of the typical conditions in **Table 1** (**Fig. 5(b3)** and **(c3)**).

The effect of the $NaBrO_3$ and MA substrate concentration on the BZ reaction can be described by the Field-Körös-Noyes (FKN) mechanism[5]. The BZ reaction process is divided into three steps in the FKN mechanism. The three steps indicate Process A of the consumption of bromide ion, Process B of the autocatalytic reaction including the oxidation of $Ru(bpy)_3^{2+}$ ($Ru(bpy)_3^{2+} \rightarrow Ru(bpy)_3^{3+}$)), and Proces C of the production of bromomalonic acid including reduction of $Ru(bpy)_3^{3+}$ ($Ru(bpy)_3^{3+} \rightarrow Ru(bpy)_3^{2+}$)). The decreased $NaBrO_3$ concentration can bring about a slow BZ reaction rate since BrO_3^- acts as a reactant in Processes A and B. Therefore, the period of BZ reaction would be increased. Similarly, the decreased MA concentration can cause a slower BZ reaction because MA can act as a reactant in Process C, resulting in a longer period. We found that SFs of the C-SOGs depended on the BZ substrate condition. The detailed dependency will be reported in our next paper. In particular, it is worth noting that the substrate-dependent SFs are similar to the ATP-dependent membrane fluctuation of the red blood cells; decreased ATP concentration causes fewer membrane fluctuations.

2.10. Supporting movies

Movie S1 Swelling/deswelling oscillation of C-SOGs (0.043) at 20 °C during the BZ reaction. Concentrations of the BZ substrates: [HNO_3] = 894 mM, [$NaBrO_3$] = 84 mM, and [MA] = 64 mM. The movie speed is 300× actual speed.

Movie S2 Swelling/deswelling oscillation of C-SOGs (0.027) at 20 °C during the BZ reaction. Concentrations of the BZ substrates: [HNO_3] = 894 mM, [$NaBrO_3$] = 84 mM, and [MA] = 64 mM. The movie speed is 300× actual speed.

Movie S3 Swelling/deswelling oscillation of C-SOGs (0.013) at 20 °C during the BZ reaction. Concentrations of the BZ substrates: [HNO_3] = 894 mM, [$NaBrO_3$] = 84 mM, and [MA] = 64 mM. The movie speed is 300× actual speed.

Movie S4 Swelling/deswelling oscillation of solid SOGs at 20 °C during the BZ reaction. Concentrations of the BZ substrates: [HNO_3] = 894 mM, [$NaBrO_3$] = 84 mM, and [MA] = 64 mM. The movie speed is 300× actual speed.

Movie S5 Swelling/deswelling oscillation of C-SOGs (0.027) at 20 °C during the BZ reaction. Concentrations of the BZ substrates: [HNO_3] = 894 mM, [$NaBrO_3$] = 42 mM, and [MA] = 64 mM. The movie speed is 300× actual speed.

Movie S6 Swelling/deswelling oscillation of C-SOGs (0.027) at 20 °C during the BZ reaction. Concentrations of the BZ substrates: [HNO_3] = 894 mM, [$NaBrO_3$] = 84 mM, and [MA] = 32 mM. The movie speed is 300× actual speed.

3. References

1   B. C. Zarket and S. R. Raghavan, *Nat. Commun.*, 2017, **8**, 193

2   Q. Chen, S. Utech, D. Chen, R. Prodanovic, J. M. Lin and D. A. Weitz, *Lab Chip*, 2016, **16**, 1346–1349.

3   I. C. Chen, O. Kuksenok, V. v. Yashin, A. C. Balazs and K. J. van Vliet, *Adv. Funct. Mater*, 2012, **22**, 2535–2541.

4   R. Yoshida, M. Tanaka, S. Onodera, T. Yamaguchi and E. Kokufuta, *J. Phys. Chem. A*, 2000, **104**, 7549–7555.

5   R. J. Field and R. M. Noyes, *J. Chem. Phys.*, 1974, **60**, 1877–1884.